Inorganic Chemistry Communications 118 (2020) 107981

Contents lists available at ScienceDirect

Inorganic Chemistry Communications

journal homepage: www.elsevier.com/locate/inoche

Short communication

Crystal structure, physical study and Hirshfeld surface analysis of $(C_9H_{26}N_4)[SnCl_6]Cl_2{\cdot}2H_2O$

Brahim El Bali[a,*], Mohammed Lachkar[b], Amani Direm[c], Michal Dusek[d], Marco Amores[e]

[a] Independent Scientist, Department of Chemistry, Faculty of Sciences, University Sidi Mohamed Ben Abdellah, B.P.1796 (Atlas), 30000 Fès, Morocco
[b] Laboratory of Ingenierie of Organometallic and Molecular Materials (LIMOM), Department of Chemistry, Faculty of Sciences, University Sidi Mohamed Ben Abdellah, B. P.1796 (Atlas), 30000 Fès, Morocco
[c] Laboratory of Structure, Properties and Intermolecular Interactions LASPI2A, Department of Matter Sciences Abbes Laghrour University, Khenchela 40.000, Algeria
[d] Institute of Physics of the Czech Academy of Sciences, Na Slovance 2, 182 21 Praha 8, Czech Republic
[e] Department of Chemistry, Graduate School of Science, The University of Tokyo, 7-3-1, Hongo, Bunkyo-Ku, Tokyo 113-0033, Japan

GRAPHICAL ABSTRACT

Hirshfeld surface illustrating the presence of the shortest reciprocal C—HC… HC—C/C—HC… HC—C interactions. Galvanostatic cycling of the $(C_9H_{28}N_4)[SnCl_6]Cl_2{\cdot}2H_2O$ at a constant current of 100 mA g^{-1} with potential limitation between 0.30 and 2.5 V.

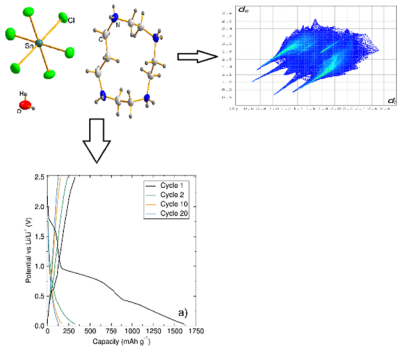

ARTICLE INFO

Keywords:
Tin-tetraazacyclotridecane
Crystal structure
Raman
Hirshfeld surface analysis
Battery application

ABSTRACT

$(C_9H_{26}N_4)[SnCl_6]Cl_2{\cdot}2H_2O$ has been synthesized in solution and its structure confirmed by single-crystal X-ray diffraction. It crystallizes in the monoclinic system, with space group $P2_1/n$ (14), Z = 4, with refined cell parameters (Å,°) a = 10.7550(3), b = 15.3981(7), c = 13.8750(5), β = 103.095(3), V = 2238.04(15) $Å^3$. The 3D framework of the title compound is made of free molecules 1,4,7,10-tetraazacyclotridecane, $[SnCl_6]$, Cl atoms and water molecules, interacting through an intricate network of hydrogen-bonds and H…Cl interactions. The 1,4,7,10-tetraazacyclotridecane moiety is also confirmed by Raman spectroscopy. The Hirshfeld surface analysis of $(C_9H_{26}N_4)[SnCl_6]Cl_2{\cdot}2H_2O$ is elucidated. Preliminary investigations of the electrochemical performance of the title compound as an active material in a Li-ion battery have also been carried out.

1. Introduction

Macrocycles are synthetic or natural polydentate ligands, with their donor atoms incorporated in a cyclic backbone or/and in substituents attached to it. They contain a cyclic framework of at least twelve atoms. Naturally occurring macrocycles can however reach even more than 50

* Corresponding author.
E-mail address: b_elbali@yahoo.com (B. El Bali).

https://doi.org/10.1016/j.inoche.2020.107981
Received 1 April 2020; Received in revised form 25 April 2020; Accepted 12 May 2020
Available online 26 May 2020
1387-7003/

Table 1
Crystal data and structure refinement details for $(C_9H_{26}N_4)[SnCl_6]Cl_2{\cdot}2H_2O$.

CCDC number	**1,990,766**
Empirical formula	$(C_9H_{26}N_4)[SnCl_6]Cl_2{\cdot}2H_2O$
Formula weight	626.7 g mol^{-1}
Temperature	293 K
Wavelength	0.71073 Å
Crystal system, space group	Monoclinic, *P*21/*n*
Unit cell dimensions	a = 10.7550 (3) Å b = 15.3981 (7) Å c = 13.8750 (5) Å β = 103.095 (3)°
Volume, Z	2238.04 (15) $Å^3$, 4
Z, calculated density	8, 1.209 g/cm^3
Absorption coefficient	0.087 mm^{-1}
F000	1248
Crystal size	0.17 × 0.12 × 0.07 mm
Theta range for data collection	3.5°–29.7°
Limiting indices	$-13 \le h \le 13$, $-20 \le k \le 11$, $-18 \le l \le 14$
Absorption correction	Multi-scan, Tmin = 0.795, Tmax = 0.874
Reflections collected/unique	15,990/5509 (Rint = 0.028)
Refinement method*	Full-matrix least-squares on $F^{2,*}$
Data/restraints/parameters	3852/9/247
Goodness-of-fit on F2	1.30
$R[F2 > 2\sigma(F2)]$, $wR(F2)$	0.034, 0.100

* The refinement was carried out against all reflections. The conventional R-factor is always based on F. The goodness of fit as well as the weighted R-factor are based on F and F^2 for refinement carried out on F and F^2, respectively. The threshold expression is used only for calculating R-factors etc. and it is not relevant to the choice of reflections for refinement.

atoms in the largest ring. The most common naturally occurring macrocyclic scaffolds are 14-, 16-, and 18-membered frameworks [1]. Over time, other classes of macrocyclic compounds have been synthesized and/or isolated from natural sources [2]. The co-ordination chemistry of macrocyclic scaffolds, such as these compounds became a major subdivision of inorganic chemistry, while intensive search for new types of macrocycles, and the number of their applications systematically, increased since their discovery [3]. Particularly, cyclams containing 14-membered tetraamine macrocycles ([14]aneN$_4$), have been of considerable interest for medical use, given their propensity to bind strongly to a wide range of metal ions (e.g. Cr, Mn, Zn and Ru) [4]. With this class of complexes, we previousely published the synthesis and biological activities of two halocuprates complexes [Cu^{II}(1,4,8,11-tetraazacyclotetradecane)] [$CuCl_3$] and [H_4(1,4,8,11-tetrazacyclotetradecane)][Cu_2Cl_6] [5], $(C_{10}H_{28}N_4)[MnCl_4(H_2O)_2]Cl_2{\cdot}2H_2O$ [6] and $Zn(HPO_3)_2{\cdot}0.5(C_{10}H_{28}N_4)$ and $Zn_2(HPO_3)_3{\cdot}0.5(C_{10}H_{28}N_4)$ [7]. Mohan et al. reported on the synthesis of nanoparticulate $Ni(OH)_2$ films from a macrocyclic nickel(II) cyclam for the seek of Hydrogen production in microbial electrolytic cells [8]. While numerous studies have been reported on the 14-membered systems, interestingly there are only a limited number of 13-membered macrocyclic tetraamine ([13]aneN$_4$), i.e. 1,4,7,10-tetra-azacyclotridecane containing compounds structurally characterized to date. Martin et al. have published the Cu^{II}-complexes with ([13]aneN$_4$) ligands [9]. Kimura et al. reported on the crystal and solution structures of Ni^{II}-13-membered macrocyclic tetramine (1,4,7,10-tetraazacyclotridecanenickel(II)) affected by a pendent

Table 2
Fractional atomic coordinates and isotropic or equivalent isotropic displacement parameters (Å2) for $(C_9H_{26}N_4)[SnCl_6]Cl_2{\cdot}2H_2O$.

	x	*y*	*z*	*Uiso*/Ueq
Sn1	0.00912 (2)	0.252101 (14)	0.240731 (15)	0.02463 (9)
Cl1	0.68821 (8)	0.96146 (6)	0.01870 (6)	0.0396 (3)
Cl2	0.69333 (8)	0.54862 (6)	0.06389 (6)	0.0364 (3)
Cl3	−0.11103 (8)	0.15024 (6)	0.12103 (6)	0.0373 (3)
Cl4	−0.09373 (8)	0.37221 (6)	0.14120 (7)	0.0404 (3)
Cl5	0.12955 (9)	0.35189 (6)	0.35978 (6)	0.0418 (3)
Cl6	0.18161 (9)	0.25244 (6)	0.14939 (7)	0.0400 (3)
Cl7	0.11202 (9)	0.13239 (6)	0.34125 (7)	0.0424 (3)
Cl8	−0.15637 (10)	0.25132 (7)	0.32467 (8)	0.0477 (4)
O1	0.1474 (4)	0.4757 (2)	0.0969 (4)	0.0850 (18)
N1	0.9546 (3)	0.9169 (2)	0.1495 (2)	0.0372 (11)
N2	0.9896 (3)	0.5932 (2)	0.1516 (2)	0.0350 (11)
N3	0.9519 (3)	0.87443 (19)	0.4175 (2)	0.0301 (10)
C1	1.0279 (4)	0.6771 (2)	0.1129 (3)	0.0408 (14)
N4	0.9447 (3)	0.62792 (19)	0.41085 (19)	0.0279 (10)
C2	0.9531 (4)	0.7541 (2)	0.1367 (3)	0.0347 (12)
C3	1.0092 (3)	0.9006 (2)	0.3334 (2)	0.0313 (11)
C4	0.9048 (3)	0.6002 (2)	0.3052 (2)	0.0297 (11)
C5	1.0212 (4)	0.8378 (2)	0.1257 (2)	0.0396 (13)
O2	0.1533 (4)	0.0219 (2)	0.1429 (3)	0.0990 (19)
C6	1.0199 (3)	0.5844 (2)	0.2614 (2)	0.0352 (12)
C7	0.9045 (3)	0.9180 (2)	0.2411 (2)	0.0325 (12)
C8	0.9995 (3)	0.7171 (2)	0.4310 (2)	0.0288 (11)
C9	0.8959 (3)	0.7856 (2)	0.4132 (2)	0.0275 (11)
H1c1	1.117354	0.686854	0.139016	0.0489*
H2c1	1.01816	0.673038	0.042542	0.0489*
H1c2	0.942427	0.749081	0.203303	0.0416*
H2c2	0.870007	0.754558	0.092925	0.0416*
H1c3	1.063805	0.854985	0.320009	0.0375*
H2c3	1.059462	0.952116	0.350936	0.0375*
H1c4	0.851848	0.644228	0.267698	0.0357*
H2c4	0.855153	0.547919	0.300901	0.0357*
H1c5	1.106027	0.835969	0.166617	0.0475*
H2c5	1.0336	0.842166	0.059454	0.0475*
H1c6	1.086683	0.624309	0.289902	0.0422*
H2c6	1.053443	0.527391	0.279461	0.0422*
H1c7	0.83857	0.875096	0.235964	0.039*
H2c7	0.865879	0.973316	0.247224	0.039*
H1c8	1.057588	0.72825	0.389092	0.0345*
H2c8	1.047388	0.720535	0.498285	0.0345*
H1c9	0.840021	0.776541	0.349533	0.033*
H2c9	0.846284	0.780351	0.462372	0.033*
H1n3	1.013 (2)	0.877 (2)	0.4694 (16)	0.0361*
H1n4	0.880 (2)	0.621 (2)	0.436 (2)	0.0334*
H1n1	0.887 (2)	0.921 (2)	0.103 (2)	0.0446*
H2n4	1.004 (2)	0.5921 (18)	0.437 (2)	0.0334*
H2n1	1.012 (3)	0.9555 (19)	0.150 (3)	0.0446*
H1n2	1.036 (3)	0.5573 (19)	0.128 (2)	0.0419*
H2n3	0.894 (3)	0.9124 (18)	0.418 (2)	0.0361*
H2n2	0.9094 (14)	0.590 (2)	0.126 (2)	0.0419*
H2o1	0.187 (5)	0.480 (3)	0.059 (4)	0.1019*
H1o1	0.140 (5)	0.427 (2)	0.103 (4)	0.1019*

phenol [10], while the electrochemical behaviour of that same complex was reported in [11]. Kimura et al. studied the oxidation behavior of square-planar 13-15_membered macrocyclic tetraamine complexes of M^{+2}, M = Ni and Cu [12]. The polarographic study on the Cu^{II}-1,4,7,10-tetra-azacyclotridecane complex was reported by Kodama and

Table 3
Geometric parameters (Å, °) for $(C_9H_{26}N_4)[SnCl_6]Cl_2{\cdot}2H_2O$.

Bond lenght (Å)		Bond lenght (Å)	
Sn1−Cl3	2.4323 (9)	C1−H1c1	0.96
Sn1−Cl4	2.4205 (9)	C1−H2c1	0.96
Sn1−Cl5	2.4078 (9)	N4−C4	1.493 (4)
Sn1−Cl6	2.4725 (11)	N4−C8	1.496 (4)
Sn1−Cl7	2.4225 (9)	N4−H1n4	0.86 (3)
Sn1−Cl8	2.3375 (12)	N4−H2n4	0.86 (3)
Cl1−N1	3.100 (3)	C2−C5	1.507 (5)
Cl1−N4^{i}	3.194 (3)	C2−H1c2	0.96
Cl1−N4^{ii}	3.036 (3)	C2−H2c2	0.96
Cl2−N2	3.217 (3)	C3−C7	1.526 (4)
Cl2−N3^{iii}	3.143 (3)	C3−H1c3	0.96
Cl2−N3^{ii}	3.144 (3)	C3−H2c3	0.96
O1−H2o1	0.76 (6)	C4−C6	1.518 (5)
O1−H1o1	0.76 (4)	C4−H1c4	0.96
N1−C5	1.488 (5)	C4−H2c4	0.96
N1−C7	1.489 (5)	C5−H1c5	0.96
N1−H1n1	0.86 (2)	C5−H2c5	0.96
N1−H2n1	0.86 (3)	C6−H1c6	0.96
N2−C1	1.493 (5)	C6−H2c6	0.96
N2−C6	1.489 (4)	C7−H1c7	0.96
N2−H1n2	0.86 (3)	C7−H2c7	0.96
N2−H2n2	0.856 (15)	C8−C9	1.513 (5)
N3−C3	1.494 (5)	C8−H1c8	0.96
N3−C9	1.490 (4)	C8−H2c8	0.96
N3−H1n3	0.86 (2)	C9−H1c9	0.96
N3−H2n3	0.86 (3)	C9−H2c9	0.96
C1−C2	1.510 (5)		

Symmetry codes: (i) $-x + 3/2, y + 1/2, -z + 1/2$; (ii) $x - 1/2, -y + 3/2, z - 1/2$; (iii) $-x + 3/2, y - 1/2, -z + 1/2$; (iv) $x + 1/2, -y + 3/2, z + 1/2$.

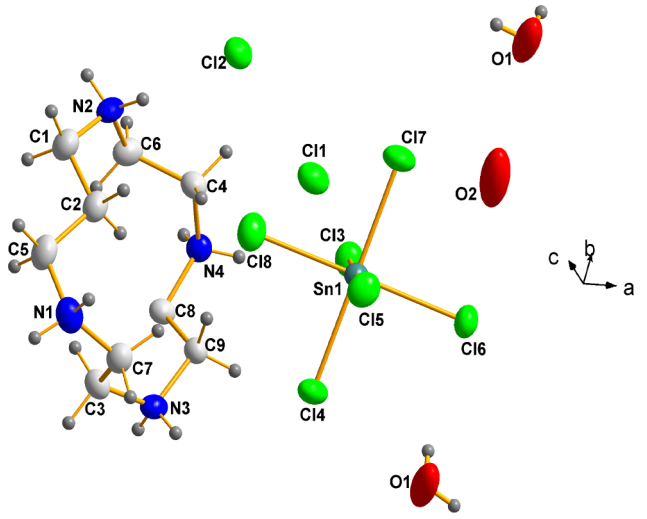

Fig. 1. . Unit cell in the crystal structure of $(C_9H_{26}N_4)[SnCl_6]Cl_2{\cdot}2H_2O$ (Thermal ellipsoids are shown at 50% probability).

Kimura [13]. The behaviour of the oxidation of the Ni(II) and Cu(II) complexes with 13- and 14-membered macrocycles have been investigated [14]. However, compared to the research reported on cyclams [15 and references herein], there is only few studies which deal with 1,4,7,10-tetraazacyclotridecane complexes, one important application was its use as ligand in radiopharmaceutical chemistry [15].

In addition, the presence of Sn in the structure could enable redox activity of the material as negative electrode for Li-ion batteries.

The present study deals with the synthesis, crystal structure, Raman and electrochemical studies of the(1,4,7,10-tetraazacyclotridecane hexachlorostannate(IV) dichloride dihydrate) $(C_9H_{26}N_4)[SnCl_6]Cl_2{\cdot}2H_2O$.

2. Experimental

2.1. Synthesis

Single crystals of $(C_9H_{26}N_4)[SnCl_6]Cl_2{\cdot}2H_2O$ (1,4,7,10-tetraazacyclotridecane hexachlorostannate(IV) dichloride dihydrate) were obtained by recrystallisation from a solution made of SnF_2 (0.1242 g) (Sigma-Aldrich 99%) and 0.0128 g [13]aneN_4 [Alfa Aesar GmbH & Co KG (Karlsruhe, Germany), $C_9H_{22}N_4$, Mr = 186.6 g/mol] dissolved in 5 mL distilled water. 2–3 drops of Metformin (1,1-Dimethylbiguanide hydrochloride), $(NH_2C(=NH)NHC(=NH)N(CH_3)_2{\cdot}HCl$, Mr = 165.62 g/mol, Sigma-Aldrich 97%) were added and a white precipitate formed. The later was dissolved by few drops of concentrated hydrochloric acid (HCl) and the mixture was stirred for 2 h before being left at ambient (P, T) conditions. After two weeks, colorless crystals formed, which were washed with the mixture Ethanol-water (w/w 80:20) and dried at air.

2.2. X-ray intensity data collection procedure

A suitable crystal (0.17 × 0.12 × 0.07) mm^3 was selected and mounted on a four-circles diffractometer Gemini of Oxford Diffraction (now Rigaku Oxford Diffraction), using graphite monochromatized MoKα radiation (λ = 0.7173 Å) collimated with Mo-Enhance collimator, and the Atlas S1 CCD detector. A numerical absorption correction based on the crystal shape was carried out with the program CrysAlis RED [16]. The structure was solved by the Direct Methods procedure of SIR97 [17] and refined by a full-matrix least-squares minimisation based on F^2 with Jana2006 [18]. The structural graphics were created using DIAMOND program [19].

The crystal data and structure refinement details are given in Table 1. The bond lengths and bond angles are given in Table 2, while the torsion angles are listed in Table 3.

CCDC 1990766 contains the supplementary crystallographic data for this paper. These data can be obtained free of charge from The Cambridge Crystallographic Data Centre via www.ccdc.cam.ac.uk/structures.

2.3. Raman spectrum

The Raman spectrum of the title compound was obtained with a Horiba Jobin Yvon LabRAM HR system equipped with a Ventus 532

Table 4
Hydrogen Bond informations in the structure of $(C_9H_{26}N_4)[SnCl_6]Cl_2{\cdot}2H_2O$ (Å, °).

D—H···*A*	*D*—H	H···*A*	*D*···*A*	*D*—H···*A*
N3—H1*n*3···Cl2^{iv}	0.86 (2)	2.38 (3)	3.144 (3)	149 (3)
N1—H1*n*1···Cl1	0.86 (2)	2.28 (2)	3.100 (3)	161 (3)
N4—H2*n*4···Cl1^{iv}	0.86 (3)	2.21 (3)	3.036 (3)	162 (2)
N1—H2*n*1···O2^{v}	0.86 (3)	1.85 (3)	2.697 (5)	169 (3)
N2—H1*n*2···O1^{vi}	0.86 (3)	1.85 (3)	2.704 (5)	171 (3)
N3—H2*n*3···Cl2^{i}	0.86 (3)	2.33 (3)	3.143 (3)	158 (2)
N2—H2*n*2···Cl2	0.856 (15)	2.375 (18)	3.217 (3)	168 (3)
O1—H2*o*1···Cl2^{vii}	0.76 (6)	2.39 (6)	3.127 (5)	164 (4)

Symmetry codes: (i) $-x+3/2, y+1/2, -z+1/2$; (iv) $x+1/2, -y+3/2, z+1/2$; (v) $x+1, y+1, z$; (vi) $x+1, y, z$; (vii) $-x+1, -y+1, -z$.

laser (λ = 532 nm), on a powdered sample between 50 and 4000 cm^{-1}, the spectral resolution is 1.42 cm^{-1}.

2.4. Galvanostatic cycling

Galvanostatic cycling measurements were conducted in a BioLogic VSP-300 potentiostat using stainless-steel Swagelok type cells. Li-metal half-cells were prepared where the working electrode consisted of a mixture of $(C_9H_{26}N_4)[SnCl_6]Cl_2{\cdot}2H_2O$ active material: conductive carbon black KET JENBACK EC-600JD (AkzoNobel):PTFE (polytetrafluoroethylene) binder (Fischer Scientific) in a 60:30:10 wt ratio pressed into a thin pellet at 2 tonnes. A 10 mm circular piece of lithium metal foil (Sigma Aldrich, ribbon, thickness × width 0.75 mm × 45 mm 99.9% trace metal basis) served as a counter and reference electrode. The electrolyte employed consisted on a 1 M solution of $LiPF_6$ salt dissolved in EC (ethylene carbonate):DMC (dimethyl carbonate) 1:1 v/v (Solvionic) soaking a glass fiber separator (Whatman GF/D). The voltage range tested during galvanostatic cycling was restrained to 0.03 and 2.50 V vs Li/Li^+ as lower and upper limits, respectively, and a constant current of 100 mA g^{-1} was applied. Specific currents used for the rate capability analyses ranged from 25 to 1000 mAh g^{-1}. In all the measurements, the mass was referred as the mass of active material present in the electrode composite.

3. Crystal structure description

The assymetric unit of the title compound $(C_9H_{26}N_4)[SnCl_6]Cl_2{\cdot}2H_2O$ consists of one molecule of the tetraprotonated 1,4,7,10-tetraazacyclotridecane ([13]aneN$_4$), two chloride anions, two water molecules and the hexachlorostannate(IV) dianion in general positions (Fig. 1).

Hydrogen atoms, those on some oxygen could not be determined because of large ADP on this water molecule. In known tetrazacycloalcanes ([13]aneN$_4$), the ligand 1,4,7,10-tetraazacyclotridecane adopts generally cavity-like conformation to engulf metal transitions as the case in M^{II}-([13]aneN$_4$) complexes [9,10]. In the title compound, $(C_9H_{26}N_4)[SnCl_6]Cl_2{\cdot}2H_2O$, the molecules of tetraazacyclotridecane are tetraprotonated and therefore are not linked to the metal in the crystal structure (Fig. 1). In fact, these molecules show no strong H-Bonds interactions, the shortest contacts being N1—H2N1.....O2^{V} interactions of 1.85(3) Å and longer as depicted in Table 4. However, considering the interactions Cl...H—C, which are enough strong, together with H...O—H from the water molecules $H_2O(1)$, to edify the 3D network in the structure of the title compound $(C_9H_{26}N_4)[SnCl_6]Cl_2{\cdot}2H_2O$ (Fig. 2).

Effectively, considering especially these interactions H…Cl, the crystal structure might be described in terms of channels along [1 0 0], where the cohesion is also reinforced by the O—H…Cl bonds. Two such channels are interconnected in the b direction through N(3)H(2)…Cl(2) interactions (Fig. 3).

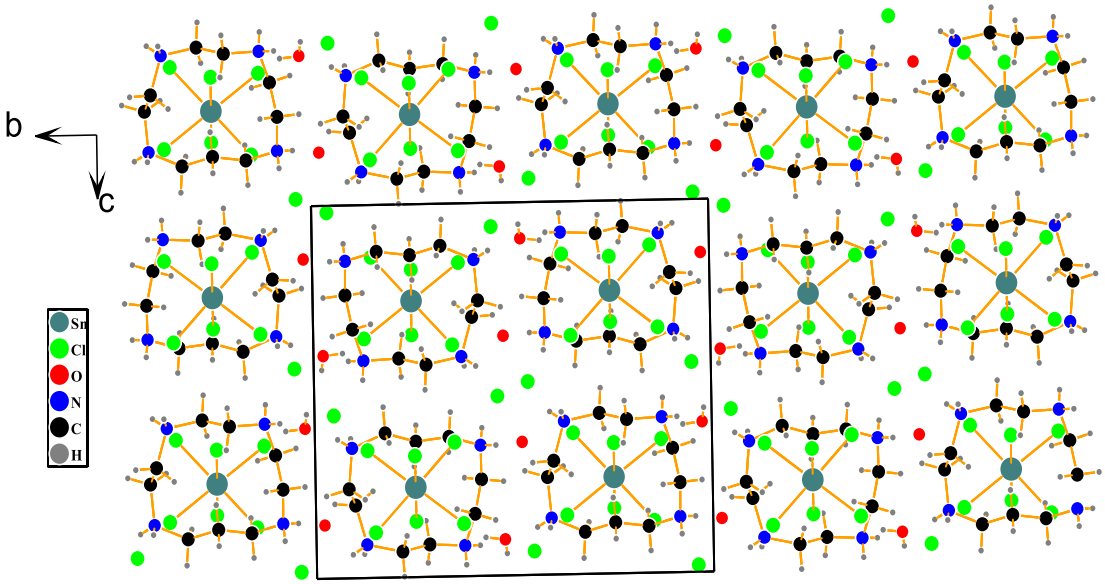

Fig. 2. The [0 1 0]-parallel chains of $(C_9H_{26}N_4)[SnCl_6]Cl_2{\cdot}2H_2O$ molecules.

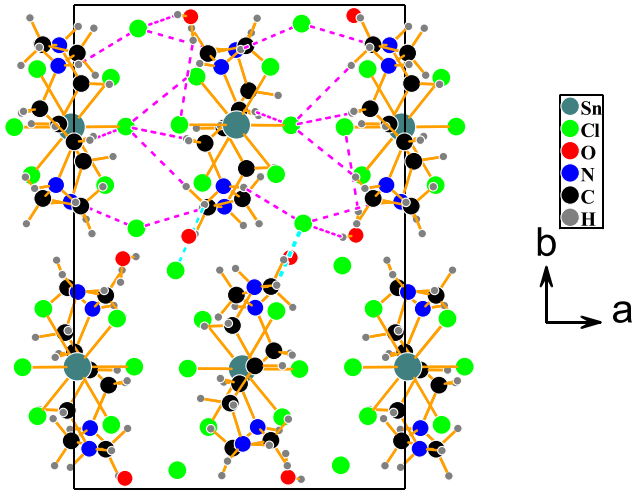

Fig. 3. Projection along [0 0 1] of the crystal structure of $(C_9H_{26}N_4)[SnCl_6]Cl_2{\cdot}2H_2O$ emphasizing the hydrogen bonding (dashed lines) inside (Pink) and between (Cyan) the chains. (For interpretation of the references to colour in this figure legend, the reader is referred to the web version of this article.)

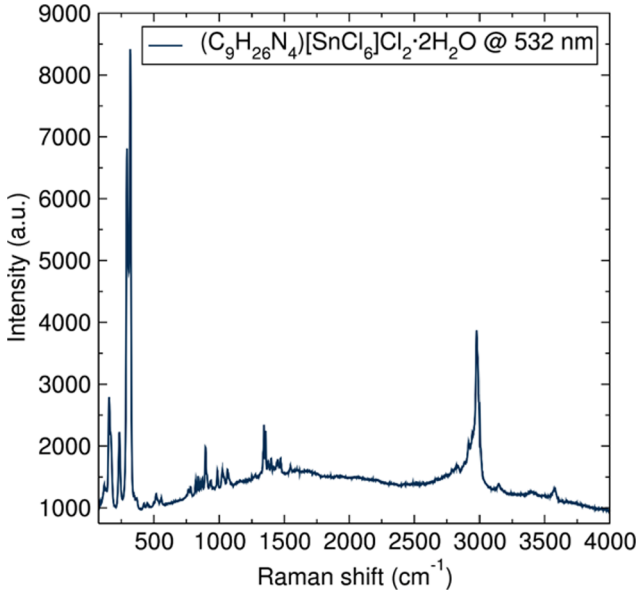

Fig. 4. Raman spectrum of $(C_9H_{26}N_4)[SnCl_6]Cl_2{\cdot}2H_2O$.

The Sn^{IV} is octacoordinated by six Cl atoms to form the octahedron $[SnCl_6]^{2-}$ in which Sn-Cl bond lengths range from 2.4078 (9) to 2.4323 (9) Å, and the axial Cl4-Sn1-Cl7 bond angle is of 179.65 (3). The bond length distortions parameter, $\Delta_{oct} = 1/6\ \Sigma[(d_i - d_m)/d_m]^2$, as defined in the literature [20,21], is of $2.8 \cdot 10^{-4}$, which indicates rather negligible distortion as behave the majority of the metals coordinated by only monodentate ligands [22].

4. Raman spectroscopy

The Raman spectrum of $(C_9H_{26}N_4)[SnCl_6]Cl_2{\cdot}2H_2O$ is depicted on Fig. 4. The spectrum is mainly described in terms of C—H and N—H modes from the 1,4,7,10-tetraazacyclotridecane molecule, while the bands 332, 329, 351, 318 cm^{-1} falling in the low-frequency region (below 300 cm^{-1}) correspond to the vibrations of the metal-ligand bonds [23,24]. In detail, Raman bands (lines) observed in the spectral range 2.830 cm^{-1} to 2.960 cm^{-1} can be assigned to symmetric and asymmetric stretching vibration of the CH_2 groups. Precisely, the weak bands located at 2.837 cm^{-1} and 2.860 cm^{-1} result from symmetric CH_2 stretching [25]. The shift at 2.959 cm^{-1} is attributed to vibrations of CH_2 groups [26], while the large band located at 2.923 cm^{-1} can be assigned to asymmetric stretching of CH_2 groups [27]. N—H stretching mode are characterized by the vibrational features observed around 3.250 cm^{-1}, but the splitting on the corresponding band in two components (3.230 cm^{-1} and 3.260 cm^{-1}) is an indication of non quivalency between the local environment of the bonded hydrogen atoms [28]. The existence of Sn—Cl groups can contribute to the shift of the N—H vibrational band due to Cl···H interactions. Referring to the literature [23,24], the fingerprint region of the spectrum (400 to 1600 cm^{-1}) contains characteristic bands assigned to general ligand vibrations, for example stretching and tetraazacyclotridecane polyamine vibrations, similar to the pyrrole in reference [23]. C—N vibrations can be present near 1200–1500 cm^{-1} region and C—C Vibrations around 750–1200 cm^{-1} together with ring breathing.

5. Hirshfeld surface analysis of $(C_9H_{26}N_4)[SnCl_6]Cl_2{\cdot}2H_2O$

A large range of properties can be visualized on the *Hirshfeld* surface [29] using the program *CrystalExplorer* [30] including the distance of atoms external, *d*e, and internal, *d*i, to the surface. The intermolecular distance information encrypted in the *Hirshfeld* surface can be condensed into a two-dimensional histogram of *d*e and *d*i, which is a unique identifier for molecules in a crystal structure, called a fingerprint plot [31,32] (Fig. 5). Instead of plotting *d*e and *d*i on the *Hirshfeld* surface, the contact distances are normalized in the *CrystalExplorer* program using the van der Waals radius of the appropriate internal and external atom of the surface, in such a way that the normalized contact distances d_{norm} [33,34] could be derived as follows:

$$d_{norm} = \frac{d_i - r_i^{vdW}}{r_i^{vdW}} + \frac{d_e - r_e^{vdW}}{r_e^{vdW}}$$

The value of dnorm is negative or positive when the intermolecular contacts are shorter or longer than the van der Waals radii, respectively. Thus, close intermolecular distances are characterized by three identically colored regions when the d_{norm} representation is mapped on the *Hirshfeld* surface.

To provide further insights into the intermolecular contacts within the crystal structure packing of the title complex and to quantify them, the *Hirshfeld* surface analysis was performed and the partial 2D-fingerprint plots were established, which showed that the complex crystal structure is governed by the following intermolecular contacts; Cl…H/H…Cl, O…H/H…O, H…H, Cl…Cl, Cl…O/O…Cl and O…O.

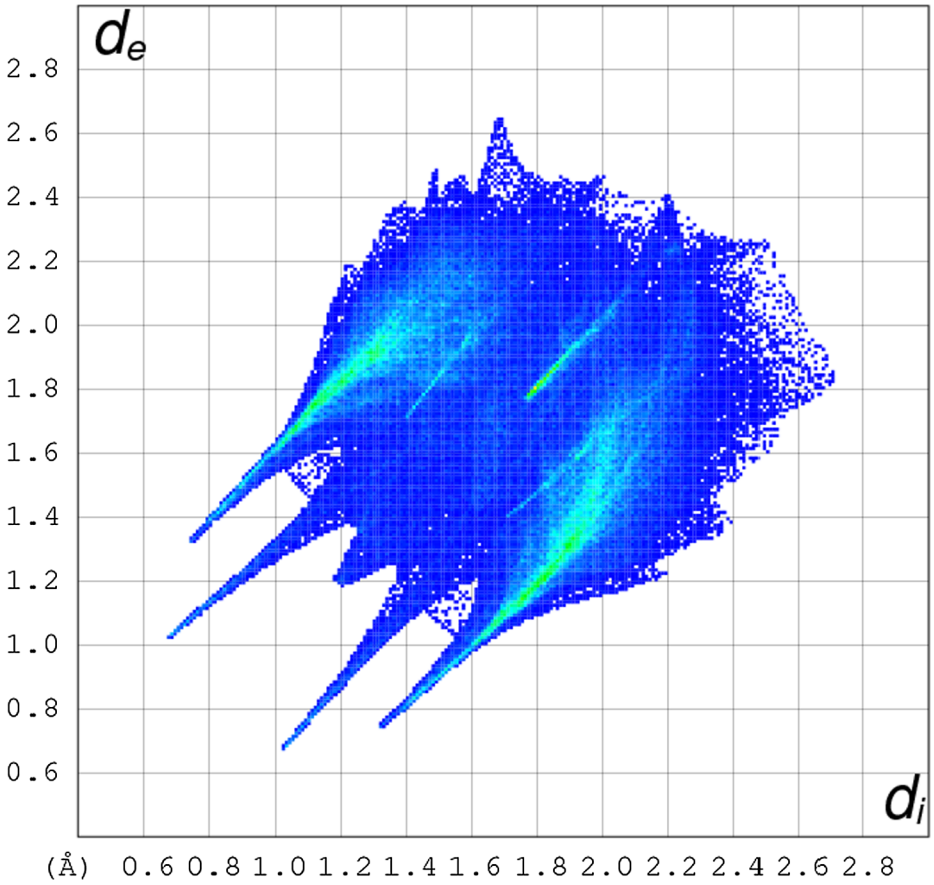

Fig. 5. Full fingerprint resulting from the overlapping of the different contacts types in the title complex.

After establishing the decomposed fingerprint plots into the separated intermolecular contacts, it can be globally noticed that the H…Cl/Cl…H intermolecular contacts are the most abundant in the crystal packing of the title complex with a 70.0% contribution (Fig. 6a). These contacts are indeed attributed to C—H…Cl, O—H…Cl and N—H…Cl interactions, which show a close contact appearing at about (*di* = 1.32 Å, *de* = 0.74 Å and *di* = 0.74 Å, *de* = 1.32 Å) and resulting from the strong Cl1… H2n4—N4/N4—H2n4…Cl1 reciprocal hydrogen-bonds (Fig. 6) [35].

Furthermore, the H…O/O…H reciprocal contacts represented by the two long symmetric spikes in the middle of the 2D-fingerprint plot (Fig. 5) are the second most frequent interactions due to the abundance of hydrogen on the molecular surface (Fig. 6c). They account for 13.0% of the total *Hirshfeld* surface (Fig. 6b). Surface that have been mapped over d_{norm} illustrated in (Fig. 6c) exhibits a big red spot associated to the reciprocal O2… H2n1—N1/N1—H2n1…O2 interactions, which appear at a *di* + *de* value of around 1.7 Å.

It is worth to be noted that the results from the 2D-fingerprint plots reveal that the contribution of the H…H contacts to the structural stability is 11.2% (Fig. 7a). They are one of the major contributors to the packing of the title compound owing to the presence of extensive networks of C—H…H—C and C—H…H—O contacts. It can be noticed from the decomposed bidimensional fingerprint that the H…H contacts, represented as a scattered points distribution and covering the most area in the total fingerprint plot, show a closest contact of 2.4 Å. The evidence of the C7-H2c7…H2c4-C4 intermolecular interaction related to this contact was made clear by establishing the *Hirshfeld* surface mapped over the *di* function in the range 0.67–2.72 Å (Fig. 7b).

Additionally, as illustrated in (Fig. 8a and b), the relative contributions of Cl…Cl and Cl…O/O…Cl contacts to the overall fingerprint plot are quite similar; 2.7% and 2.6%, respectively.

Thus drawing the *curvedness* representation on *Hirshfeld* surface ranging from −4.00 to 0.40 Å (Fig. 8c) allowed us to highlight the presence of a shortest Cl…Cl contact resulting from the *lp*…*lp* interaction between the lone pairs of the atoms Cl2 and Cl8, which has a distance of about 3.56 Å.

Concerning the O…O contacts, they represent only 0.6% of the total *Hirshfeld* surface (Fig. 9), which suggests that the attributed *lp*…*lp*

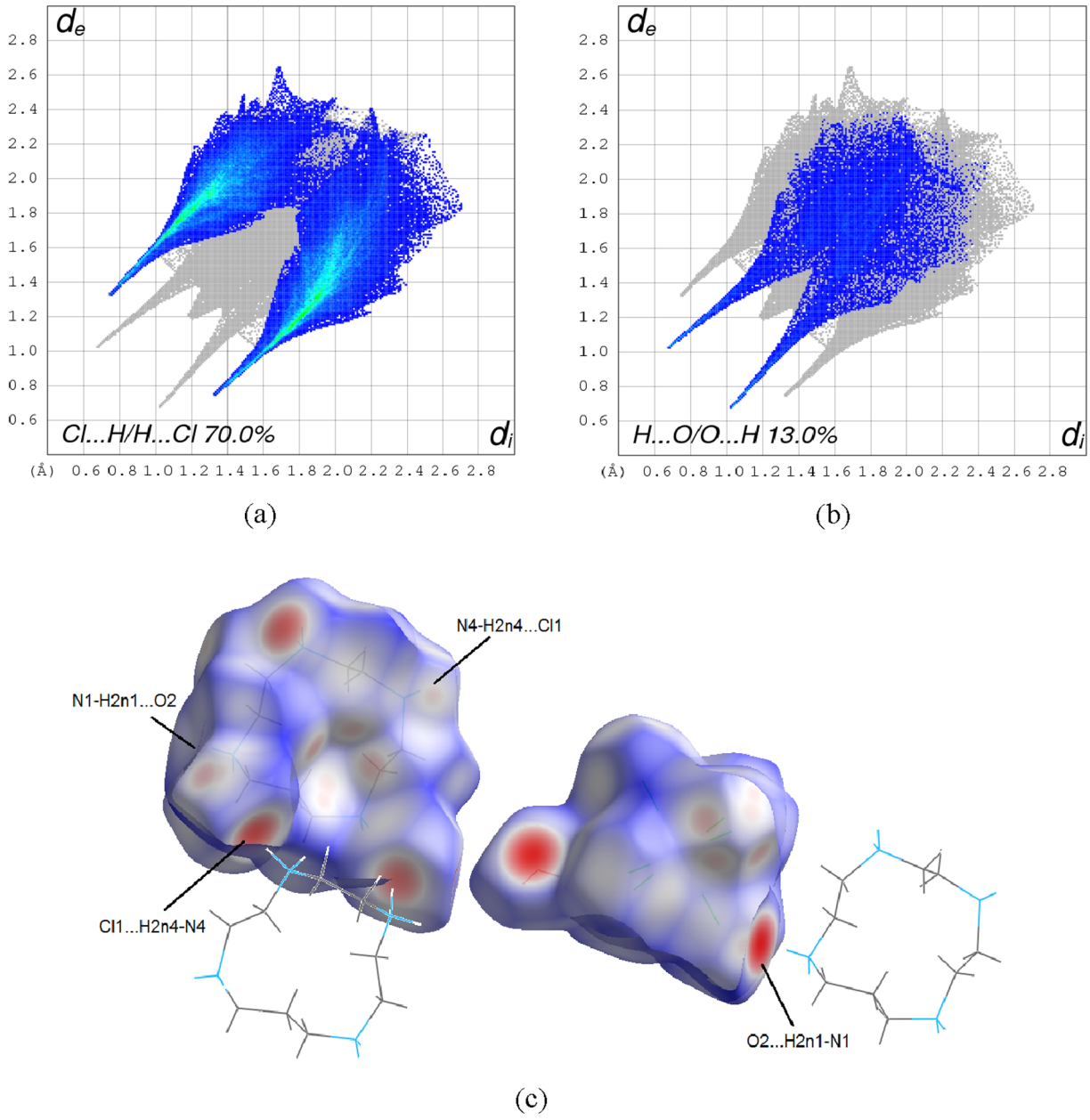

Fig. 6. Decomposed fingerprint plots into the separated intermolecular (a) H…Cl/Cl…H and (b) H…O/O…H contacts. (c) *Hirshfeld* surface environment mapped with d_{norm} over the range −0.70 to 1.14, showing the shortest Cl… H−N/N−H…Cl and O… H−N/N−H…O interactions.

interactions resulting from the oxygeńs lone pairs do not belong to the driving forces in the crystal packing formation and this is due to the limited number of oxygen atoms in the crystal structure.

Fig. 10 illustrates a schematic representation of the percentage contributions to the *Hirshfeld* area of the various intermolecular contacts present in the crystal structure of the title compound.

6. Galvanostatic cycling as negative electrode for Li-ion batteries

Sn-containing compounds typically possess redox couples below 2 V vs Li/Li^+, making them suitable materials as negative electrode for Li-ion batteries, where current graphite anodes possess safety concerns due to possible Li plating and dendrite formation at high charging rates [36-38]. The electrochemical properties of the ($C_9H_{26}N_4$)

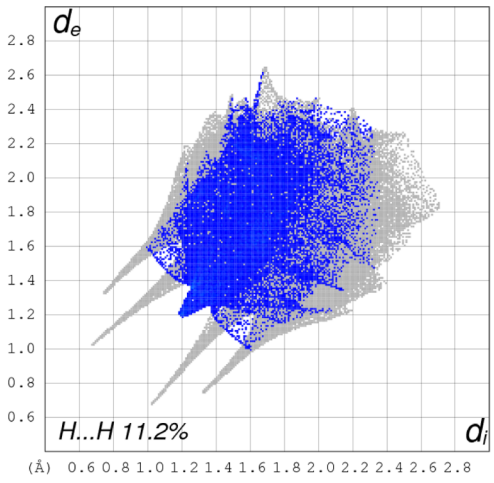

(a)

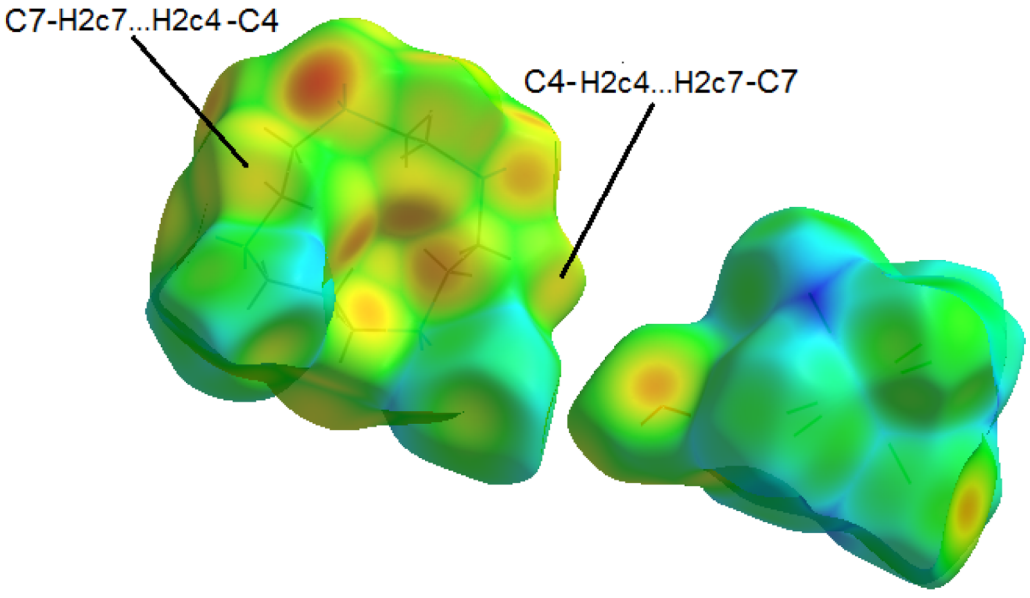

(b)

Fig. 7. . (a) Partial fingerprint plot of the intermolecular H… H contacts. (b) *Hirshfeld* surface mapped over *di* and illustrating the presence of the shortest reciprocal C7—H2c7… H2c4—C4/ C4—H2c4… H2c7—C7 interactions.

$[SnCl_6]Cl_2{\cdot}2H_2O$ as an anode material for Li-ion batteries have been analysed by galvanostatic cycling of the compound in Li-metal half-cells. The voltage profile of the cycled compound at 0.1 A g^{-1} in the 0.30–2.5 V voltage range is shown in Fig. 11a.

The voltage profile of the galvanostatic cycling shows an initial first discharge capacity above 1600 mAh g^{-1} with three main pseudo plateaus at *ca.* 1.7, 0.9 and 0.4 V. The first pseudo plateau at 1.7 V is completely irreversible and not observable in subsequent cycles. This plateau could originate from irreversible electrochemically driven decomposition *via* reduction redox processes [39]. Electrochemically driven solid-state amorphisation by lithium at low voltages is commonly observed in other Sn-containing materials such as the high capacity SnO_2 anode material [40]. The second pseudo plateau at *ca.* 0.9 V is due to SEI formation promoted by partial decomposition of the

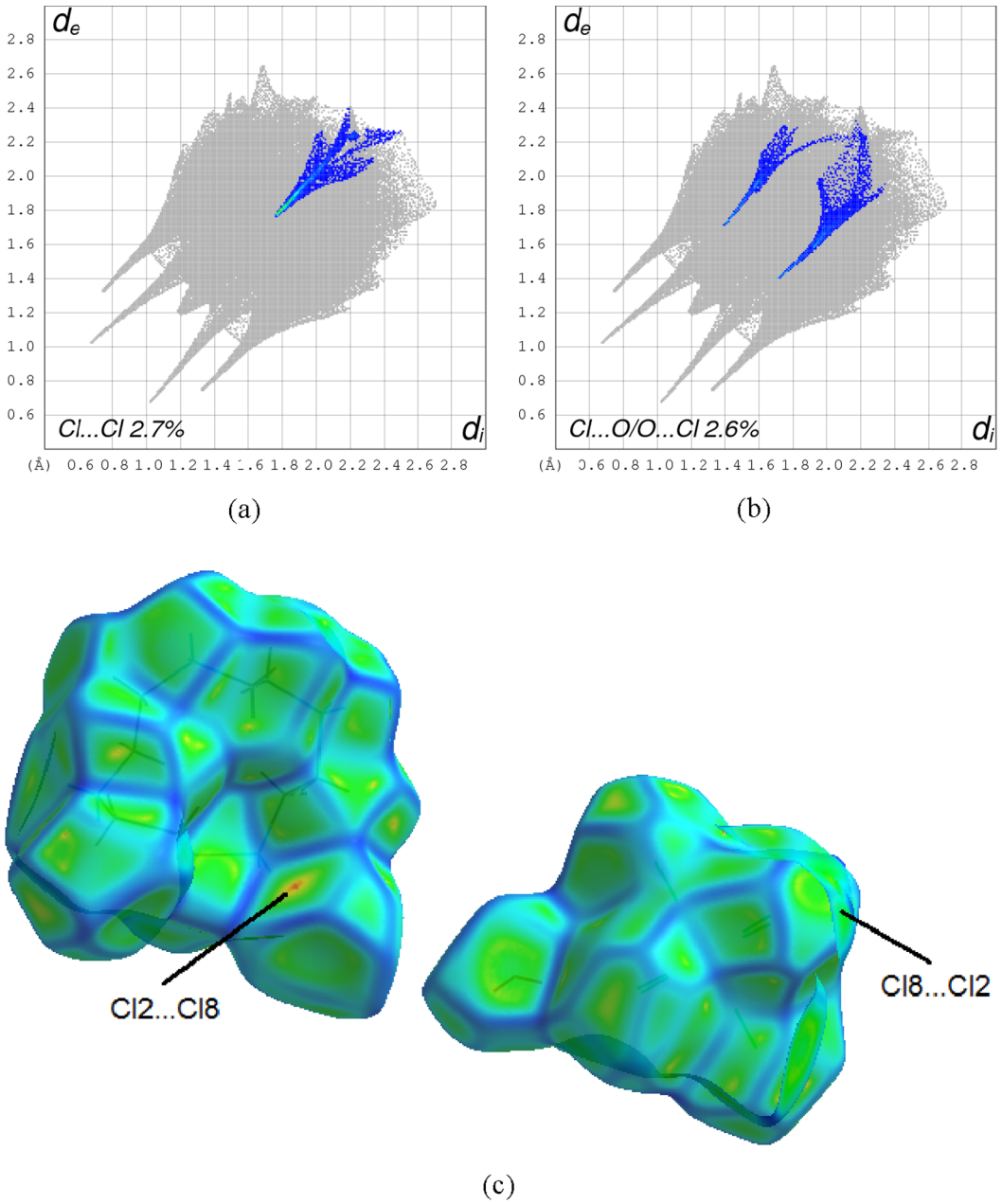

Fig. 8. Decomposed fingerprint plots into the intermolecular (a) Cl…Cl and (b) Cl…O/O…Cl contacts. (c) Curvedness representation of the Hirshfeld surface highlighting the lp…lp interactions resulting from the Cl…Cl contacts.

electrolyte on the working electrode surface, which is then stabilised after the first discharge [41]. The third observable pseudo plateau at a low voltage below 0.4 V, delivering an additional capacity near 750 mAh g^{-1} could be related to the redox reduction of tin, further decomposition processes or contributions from the conductive carbon black at low voltages. The irreversibility of the first discharge and the polarisation between charge and discharge voltages may indicate conversion or alloying processes, but the exact reduction mechanism is

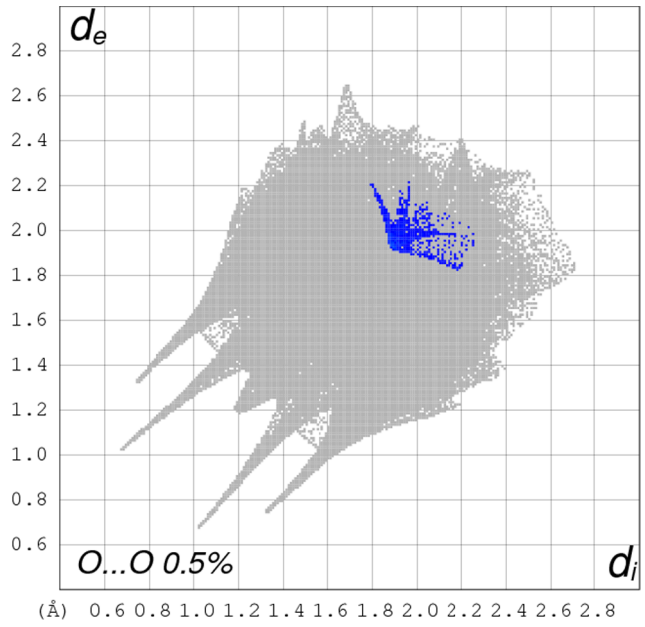

Fig. 9. Decomposed fingerprint plot of the corresponding O…O contacts.

unclear and requires further characterisations [42-44]. A similar discharge profile has been observed for the Sn_2PO_4Cl material, with an irreversible plateau noted below 1.8 V and a reversible plateau below 0.5 V. The nature of these plateaus is attributed in that case to the presence of phosphate and chloride moieties which preclude intercalation in favour of formation of metallic Sn and subsequent alloy processes [45]. During cell charging, clear plateaus can be observed below 1 V, specifically at 0.6 V, 0.75 and 0.82 V.

Looking at the diffrential capacity profiles, several reduction peaks can be observed at 1.7, 0.9, 0.6 and 0.4 V. (Fig. 11b). From these peaks, the redox processes at 0.6 and 0.4 V appear to be reversible during charging and be also present on the second cycle. In the oxidation sweep, three peaks can be observed at 0.6 V, 0.75 and 0.82 V which appear reversible as they are also present in the second cycle, although with capacity contribution. The sharpness of the oxidation peak at 0.6 V indicates the presence of plateau-like features in the galvanostatic cycling, indicative of two-phase transformation processes. Further characterisation such as *in-operando* PXRD would be required to confirm this phenomenon.

The capacity retention and coulombic efficiency is shown in Fig. 12. A capacity above 125 mAh g^{-1} is retained after 20 cycles of galvanostatic cycling at 100 mA g^{-1} with a coulombic efficiency above 95% achieved after 20 cycles. Due to the instability of the electrolyte at low voltages and possible SEI dissolution/reformation, parasitic reactions could be taking place during cycling and affect the columbic efficiency of the cell.

The rate capability of the material was also studied by cycling a fresh cell at different current rates (Fig. 13). The material displays a modest rate capability, without extreme capacity loses when increasing the current rate, delivering discharge capacities near 75 mAh g^{-1} at 1 A g^{-1}. The material also possesses good capacity retention when returning to the initial value of 25 mA g^{-1} with a capacity above 225 mAh g^{-1}.

These studies analyse the redox activity of the $(C_9H_{26}N_4)[SnCl_6]Cl_2{\cdot}2H_2O$ compound when tested as negative electrode in a Li-ion battery. The observed redox activity can be preliminarily attributed to the presence of Sn^{+4} cations in the crystal structure.

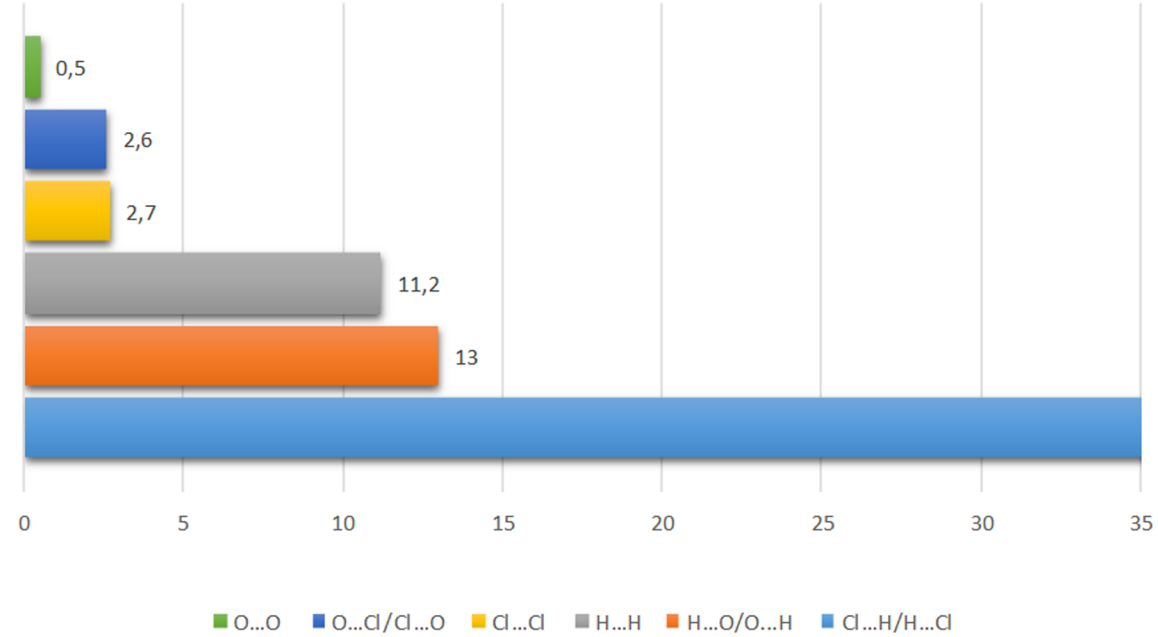

Fig. 10. . Schematic illustration of the decomposed fingerprint plots into the different contacts within the title compound.

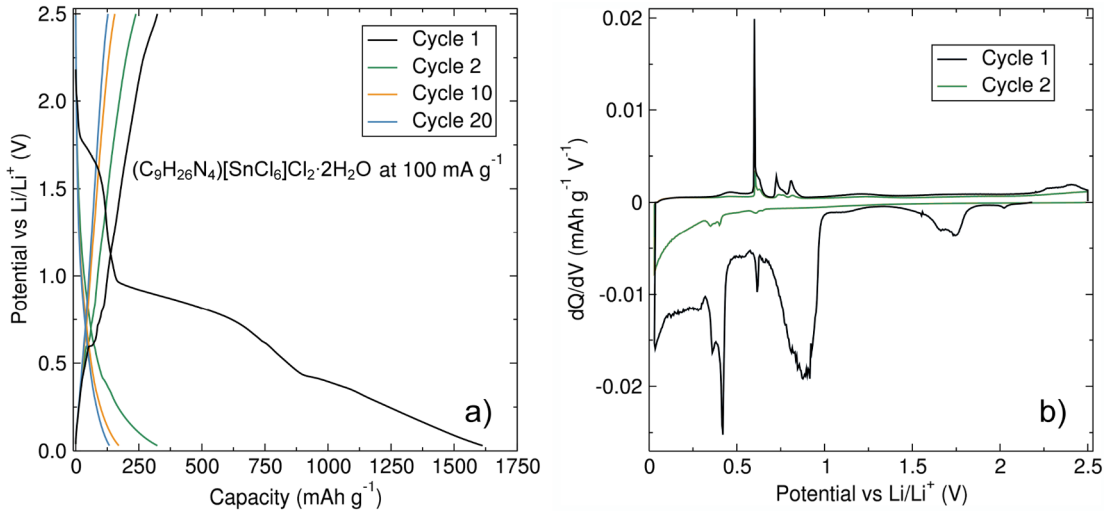

Fig. 11. . (a) Galvanostatic cycling of the $(C_9H_{26}N_4)[SnCl_6]Cl_2{\cdot}2H_2O$ compound at a constant current of 100 mA g^{-1} with potential limitation between 0.30 and 2.5 V. (b) Differential capacity plot of the first two galvanostatic cycles where redox responses towards electrochemical reaction with Li ions can be identified at specific voltages.

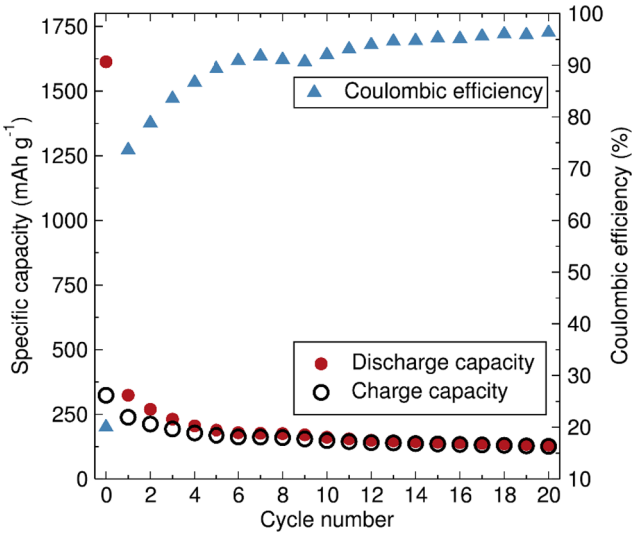

Fig. 12. Capacity retention during the first 20 cycles from galvanostatic cycling of the $(C_9H_{26}N_4)[SnCl_6]Cl_2{\cdot}2H_2O$ compound at 100 mA g^{-1} and the corresponding columbic efficiencies for each cycle.

7. Conclusions

$(C_9H_{26}N_4)[SnCl_6]Cl_2{\cdot}2H_2O$ has been synthesized in solution and its structure confirmed by single-crystal X-ray diffraction. Its 3D framework of the title compound is made of tetraazacyclotridecane polyamine molecules, $[SnCl_6]$, Cl atoms and water molecules, interacting through an intricate network of hydrogen-bonds and H…Cl interactions. The macrocyclic moiety is also confirmed using Raman spectroscopy. The Hirshfeld surface analysis of $(C_9H_{26}N_4)[SnCl_6]Cl_2{\cdot}2H_2O$ is elucidated and correlated to the crystal structure data. Preliminary investigations of the electrochemical performance of the title compound as an active material in a Li-ion battery are commented.

8. Authors contributions statement

B. El Bali synthesized the crystals and designed the manuscript. M. Dusek solved the crystal structure and corrected the structural part. A. Direm wrote the Hirshfeld surface analysis part. Marco Amores wrote the galvanostatic part. M. Lachkar revised the manuscript.

Declaration of Competing Interest

The authors declare that they have no known competing financial interests or personal relationships that could have appeared to influence the work reported in this paper.

Acknowledgements

The crystallographic part was supported by the project 18-10438S of the Czech Science Foundation using instruments of the ASTRA laboratory established within the Operation program Prague Competitiveness - project CZ.2.16/3.1.00/24510. Brahim would thank Prof. F. Chandad (Faculty of dentisery, Laval University, Québec, Canada) to have provided benevolently the 1,4,7,10-tetraazacyclotridecane reactant. The galvanostatic measurements were achieved in thanks to Prof. Serena Corr (Department of Chemical and Biological Engineering, University of Sheffield, U. K.).

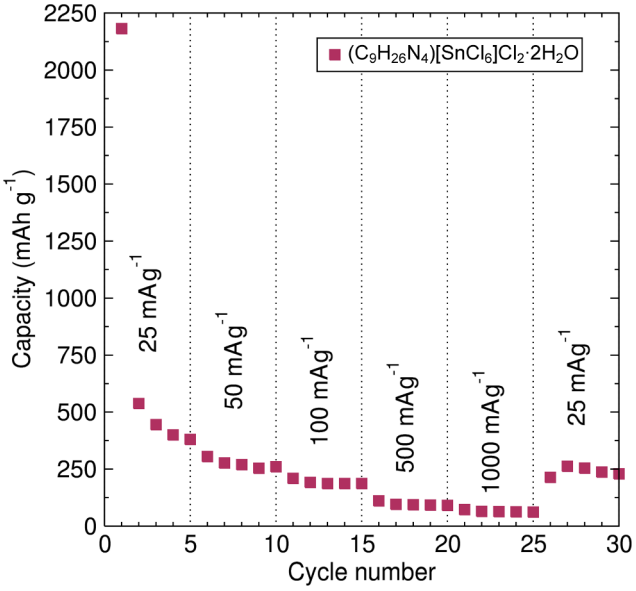

Fig. 13. Rate capability analyses of the $(C_9H_{26}N_4)[SnCl_6]Cl_2{\cdot}2H_2O$ compound at specific currents between 25 mA g^{-1} and 1 A g^{-1}. The first cycle with a high irreversible discharge capacity of 2172 mAh g^{-1} has been omitted for clarity.

Appendix A. Supplementary material

Supplementary data to this article can be found online at https://doi.org/10.1016/j.inoche.2020.107981.

References

[1] A.T. Frank, N.S. Farina, N. Sawwan, O.R. Wauchope, M. Qi, E.M. Brzostowska, W. Chan, F.W. Grasso, P. Haberfield, A. Greer, Natural macrocyclic molecules have a possible limited structural diversity, Mol. Divers. 11 (2007) 115–118, https://doi.org/10.1007/s11030-007-9065-5.

[2] L.A. Wessjohann, E. Ruijter, D. Garcia-Rivera, W. Brandt, What can a chemist learn from nature's macrocycles? - A brief, conceptual view, Mol. Divers. 9 (2005) 171–186, https://doi.org/10.1007/s11030-005-1314-x.

[3] L.F. Lindoy, The Chemistry of Macrocyclic Ligand Complexes, Cambridge University Press, 1989. https://doi.org/10.1017/cbo9780511564376.

[4] X. Liang, P.J. Sadler, Cyclam complexes and their applications in medicine, Chem. Soc. Rev. 33 (2004) 246–266, https://doi.org/10.1039/b313659k.

[5] M. Lachkar, I. Halime, A. Bezgour, B. El Bali, M. Dusek, K. Fejfarova, S. Siddiq, B.P. Marasini, S. Noreen, A. Khan, S. Rasheed, M. Iqbalchoudhary, Two new halocuprates complexes $[Cu^{II}(1,4,8,11\text{-tetraazacyclotetradecane})][Cu^{I}Cl_3]$ and $[H_4(1,4,8,11\text{-tetrazacyclotetradecane})][Cu_2Cl_6]$: Synthesis, characterizations and biological studies, Med. Chem. Res. 21 (2012) 4290–4300, https://doi.org/10.1007/s00044-011-9968-7.

[6] M. Pojarová, K. Fejfarová, B. El Bali, 1,4,8,11-Tetraazoniacyclotetradecane diaquatetrachloridomanganese(II) dichloride dihydrate, Acta Crystallogr, Sect. E Struct. Reports Online. 66 (2010) m1103, https://doi.org/10.1107/S1600536810031958.

[7] I. Halime, A. Bezgour, M. Fahim, M. Dusek, K. Fejfarova, M. Lachkar, B. ElBali, Synthesis and structural characterization of two new layered inorganic-organic hybrid zinc phosphites templated by cyclam: $Zn(HPO_3)_2{\cdot}0.5(C_{10}H_{28}N_4)$ and $Zn_2(HPO_3)_3{\cdot}0.5(C_{10}H_{28}N_4)$, J. Chem. Crystallogr. 41 (2011) 223–229, https://doi.org/10.1007/s10870-010-9868-6.

[8] M. Qin, W.A. Maza, B.M. Stratakes, S.R. Ahrenholtz, A.J. Morris, Z. He, Nanoparticulate Ni(OH) 2 films synthesized from macrocyclic nickel(II) cyclam for hydrogen production in microbial electrolysis cells, J. Electrochem. Soc. 163 (2016) F437–F442, https://doi.org/10.1149/2.1081605jes.

[9] J.G. Martin, R.M.C. Wei, S.C. Cummings, Copper(II) Complexes with 13-Membered Macrocyclic Ligands Derived from Triethylenetetramine and Acetylacetone, Inorg. Chem. 11 (1972) 475–479, https://doi.org/10.1021/ic50109a010.

[10] E. Kimura, T. Koike, K. Uenishi, R.B. Davidson, Novel electrochemical behaviour of a nickel(II)-13-membered macrocyclic tetra-amine effected by a pendent phenol, J. Chem. Soc. Chem. Commun. 1110–1111 (1986), https://doi.org/10.1039/C39860001110.

[11] E. Kimura, K. Uenishi, T. Koike, Y. Iitaka, Crystal and Solution Structures of Nickel (II)-13-Membered Macrocyclic Tetramine [1,4,7,10-tetraazacyclotridecanenickel (II)] Effected by a Pendent Phenol, Chem. Lett. 15 (1986) 1137–1140, https://doi.org/10.1246/cl.1986.1137.

[12] E. Kimura, T. Koike, R. Machida, R. Nagai, M. Kodama, Effects of imide anions and axial donors on the stability and oxidation behavior of square-planar 13–15-membered macrocyclic tetraamine complexes of nickel(II) and copper(II), Inorg. Chem. 23 (1984) 4181–4188, https://doi.org/10.1021/ic00193a017.

[13] M. Kodama, E. Kimura, The 13-membered macrocyclic effect. Polarographic studies of copper(II)-1,4,7,10-tetraazacyclotridecane complexation, J. Chem. Soc. Chem. Commun. (1975) 891–892, https://doi.org/10.1039/C39750000891.

[14] M.P. Suh, S.G. Kang, Synthesis and properties of nickel(II) and copper(II) complexes of 14-membered hexaaza macrocycles, 1,8-dimethyl- and 1,8-diethyl-1,3,6,8,10,13-hexaazacyclotetradecane, Inorg. Chem. 27 (14) (1988) 2544–2546, https://doi.org/10.1021/ic00287a034.

[15] (a) R. van Eldik, C.D. Hubbard, Insights from Imaging in Bioinorganic Chemistry, in: Adv. Inorg. Chem., Elsevier, 2016: pp. 2–509. https://doi.org/10.1016/S0898-8838(16)30009-6.
(b) B.P. Burke, J. Seemann, S.J. Archibald, Advanced Chelator Design for Metal Complexes in Imaging Applications: Radiopharmaceuticals, Protein Targeting, and Conjugation, Adv. Inorg. Chem. 68 (2016) 301–339, https://doi.org/10.1016/bs.adioch.2015.11.002

[16] Agilent, CrysAlis PRO. Agilent Technologies, Yarnton, England, 2010.

[17] A. Altomare, M.C. Burla, M. Camalli, G.L. Cascarano, C. Giacovazzo, A. Guagliardi, A.G.G. Moliterni, G. Polidori, R. Spagna, SIR97: A new tool for crystal structure determination and refinement, J. Appl. Crystallogr. 32 (1999) 115–119, https://doi.org/10.1107/S0021889898007717;
L. Superflip, G. Palatinus, Chapuis, SUPERFLIP - A computer program for the solution of crystal structures by charge flipping in arbitrary dimensions, J. Appl. Crystallogr. 40 (2007) 786–790, https://doi.org/10.1107/S0021889807029238.

[18] V. Petricek, M. Dusek, L. Palatinus, Crystallographic Computing System JANA2006: General features, Z. Kristallogr. 229(5) (2014) 345-352. doi: 10.1515/zkri-2014-1737.

[19] K. Brandenburg, H. Putz, DIAMOND Version 3. Crystal Impact GbR, Postfach 1251, D-53002 Bonn, Germany, 2005.

[20] K. Robinson, G.V. Gibbs, P.H. Ribbe, Quadratic elongation: A quantitative measure of distortion in coordination polyhedra, Science 172 (1971) 567–570, https://doi.org/10.1126/science.172.3983.567.

[21] M.E. Fleet, Distortion parameters for coordination polyhedra, Mineral. Mag. 40 (1976) 531–533, https://doi.org/10.1180/minmag.1976.040.313.18.

[22] S. Alvarez, Distortion pathways of transition metal coordination polyhedra induced by chelating topology, Chem. Rev. 115 (2015) 13447–13483, https://doi.org/10.1021/acs.chemrev.5b00537.

[23] H. Ogoshi, E. Watanabe, Z. Yoshida, J. Kincaid, K. Nakamoto, Synthesis and Far-Infrared Spectra of Ferric Octaethylporphine Complexes, J. Am. Chem. Soc. 95 (1973) 2845–2849, https://doi.org/10.1021/ja00790a017.

[24] M.L. Mitchell, X.Y. Li, J.R. Kincaid, T.G. Spiro, Axial ligand and out-of-plane vibrations for bis(imidazolyl)heme: Raman and infrared iron-54, nitrogen-15, and deuterium isotope shifts and normal coordinate calculations, J. Phys. Chem. 91 (1987) 4690–4696, https://doi.org/10.1021/j100302a013.

[25] V.B. Singh, A.K. Singh, A.K. Rai, A.N. Singh, D.K. Rai, Vibrational assignment of the normal modes of 2-phenyl-4-(4-methoxy benzylidene)-2-oxazolin-5-one via FTIR and Raman spectra, and ab inito calculations, Spectrochim. Acta - Part A Mol. Biomol. Spectrosc. 67 (2007) 687–693, https://doi.org/10.1016/j.saa.2006.07.049.

[26] J. Xu, I.S. Butler, D.F.R. Gibson, I. Stangel, High-pressure infrared and FT-Raman investigation of a dental composite, Biomaterials. 18 (1997) 1653–1657, https://doi.org/10.1016/S0142-9612(97)00123-3.

[27] O. Frank, J. Jehlička, H.G.M. Edwards, Raman spectroscopy as tool for the characterization of thio-polyaromatic hydrocarbons in organic minerals, Spectrochim. Acta - Part A Mol. Biomol. Spectrosc. 68 (2007) 1065–1069, https://doi.org/10.1016/j.saa.2006.12.033.

[28] R. Smierciak, J. Passariello, E.L. Blinn, A Comparative Study of Steric Effects of Nickel(II) Complexes Containing 12-Membered Macrocyclic Ligands, Inorg. Chem. 16 (1977) 2646–2648, https://doi.org/10.1021/ic50176a046.

[29] M.A. Spackman, D. Jayatilaka, Hirshfeld surface analysis, CrystEngComm. 11 (2009) 19–32, https://doi.org/10.1039/b818330a.

[30] Wolff, S. K., Grimwood, D. J., McKinnon, J. J., Turner, M. J., Jayatilaka, D. and Spackman, M. A. (2012). CrystalExplorer 3.1, University of Western Australia: Perth, Australia.

[31] M.A. Spackman, P.G. Byrom, A novel definition of a molecule in a crystal, Chem. Phys. Lett. 267 (1997) 215–220, https://doi.org/10.1016/S0009-2614(97)00100-0.

[32] M.A. Spackman, J.J. McKinnon, Fingerprinting intermolecular interactions in molecular crystals, CrystEngComm. 4 (2002) 378–392, https://doi.org/10.1039/b203191b.

[33] J.J. McKinnon, M.A. Spackman, A.S. Mitchell, Novel tools for visualizing and exploring intermolecular interactions in molecular crystals, Acta Crystallogr. Sect. B Struct. Sci. 60 (2004) 627–668, https://doi.org/10.1107/S0108768104020300.

[34] J.J. McKinnon, D. Jayatilaka, M.A. Spackman, Towards quantitative analysis of intermolecular interactions with Hirshfeld surfaces, Chem. Commun. (2007) 3814–3816, https://doi.org/10.1039/b704980c.

[35] G.R. Desiraju, T. Steiner, The Weak Hydrogen Bond in structural chemistry and biology. IUCr Monographs on Crystallography 9, Oxford University Press, 1999. https://doi.org/10.1107/s0108768199016900.

[36] B. Wang, B. Luo, X. Li, L. Zhi, The dimensionality of Sn anodes in Li-ion batteries, Mater. Today. 15 (2012) 544–552, https://doi.org/10.1016/S1369-7021(13)70012-9.

[37] M. Zhang, T. Wang, G. Cao, Promises and challenges of tin-based compounds as anode materials for lithium-ion batteries, Int. Mater. Rev. 60 (2015) 330–352, https://doi.org/10.1179/1743280415Y.0000000004.

[38] A.R. Kamali, D.J. Fray, Tin-based materials as advanced anode materials for lithium ion batteries: A review, Rev. Adv. Mater. Sci. 27 (2011) 14–24, https://doi.org/10.

1002/adfm.202001298.
[39] P. Limthongkul, Y. Il Jang, N.J. Dudney, Y.M. Chiang, Electrochemically-driven solid-state amorphization in lithium-metal anodes, J. Power Sources. 119–121 (2003) 604–609. https://doi.org/10.1016/S0378-7753(03)00303-3.
[40] J.Y. Huang, L. Zhong, C.M. Wang, J.P. Sullivan, W. Xu, L.Q. Zhang, S.X. Mao, N.S. Hudak, X.H. Liu, A. Subramanian, H. Fan, L. Qi, A. Kushima, J. Li, In situ observation of the electrochemical lithiation of a single SnO2 nanowire electrode, Science (80-.). 330 (2010) 1515–1520. https://doi.org/10.1126/science.1195628.
[41] E. Peled, S. Menkin, Review—SEI: Past, Present and Future, J. Electrochem. Soc. 164 (2017) A1703–A1719, https://doi.org/10.1149/2.1441707jes.
[42] M.N. Obrovac, V.L. Chevrier, Alloy negative electrodes for Li-ion batteries, Chem. Rev. 114 (2014) 11444–11502, https://doi.org/10.1021/cr500207g.
[43] C. Liang, M. Gao, H. Pan, Y. Liu, M. Yan, Lithium alloys and metal oxides as high-capacity anode materials for lithium-ion batteries, J. Alloys Compd. 575 (2013) 246–256, https://doi.org/10.1016/j.jallcom.2013.04.001.
[44] J. Cabana, L. Monconduit, D. Larcher, M.R. Palacín, Beyond intercalation-based Li-ion batteries: The state of the art and challenges of electrode materials reacting through conversion reactions, Adv. Mater. 22 (2010) E170–E192, https://doi.org/10.1002/adma.201000717.
[45] F.J.F. Madrigal, C.P. Vicente, J.L. Tirado, On the Structure and Electrochemical Reactions with Lithium of Tin(II) Phosphate Chloride, J. Electrochem. Soc. 147 (2000) 1663–1667, https://doi.org/10.1149/1.1393414.